iJRASET
International Journal For Research in Applied Science and Engineering Technology

INTERNATIONAL JOURNAL FOR RESEARCH

IN APPLIED SCIENCE & ENGINEERING TECHNOLOGY

Volume: 14 **Issue:** II **Month of publication:** February 2026

DOI: https://doi.org/10.22214/ijraset.2026.77745

www.ijraset.com

Call: 08813907089 | E-mail ID: ijraset@gmail.com

International Journal for Research in Applied Science & Engineering Technology (IJRASET)
ISSN: 2321-9653; IC Value: 45.98; SJ Impact Factor: 7.538
Volume 14 Issue II Feb 2026- Available at www.ijraset.com

Advances in Gallium-Based Metal Monochalcogenide Photodetectors: From Fundamental Physics to Heterojunction Engineering

Sahin Sorifi
Department of Physics, Godda College, Godda, Sido-Kanhu Murmu University, Dumka

Abstract: ***Two-dimensional (2D) metal monochalcogenides (MMCs) have emerged as a pivotal class of semiconductors, offering unique optoelectronic properties that bridge the gaps left by graphene and transition metal dichalcogenides. This review provides a comprehensive analysis of gallium-based MMCs, specifically GaS and GaSe, detailing their evolution from fundamental material physics to advanced device applications. We begin by elucidating the core sensing mechanisms-photoconductive, photogating, and photovoltaic effects-that govern light-matter interactions in 2D systems, followed by a rigorous definition of the figures-of-merit essential for evaluating photodetector performance. The article systematically surveys contemporary synthesis strategies, contrasting top-down exfoliation methods with bottom-up growth techniques such as chemical vapor deposition (CVD), physical vapor deposition (PVD), and pulsed laser deposition (PLD). A significant focus is placed on heterojunction engineering, highlighting how the integration of Ga-based MMCs into van der Waals heterostructures and 2D/3D interfaces can enhance carrier mobility, prolong photocarrier lifetimes, and enable self-powered operation. By synthesizing the current state of research, this work underscores the transformative potential of gallium-based MMCs in the development of next-generation, high-sensitivity multispectral photodetectors.***

Keywords: 2D Materials, Metal Monochalcogenides, Gallium Selenide (GaSe), Gallium Sulphide (GaS), Photodetectors, Heterojunctions, Sensing Mechanisms, Synthesis.

I. INTRODUCTION

The isolation of graphene in 2004 marked the genesis of a revolutionary era in materials science, demonstrating that stable, atomically thin layers could exhibit extraordinary carrier mobilities and thermal conductivities [1]. However, the absence of an intrinsic bandgap in graphene remains a fundamental hurdle for its application in high-contrast optoelectronics and logic-integrated devices [2]. This limitation catalyzed a global search for two-dimensional (2D) semiconductors with tunable electronic properties, leading to the rapid characterization of transition metal dichalcogenides (TMDCs) like MoS_2 [3] and WS_2 [4]. While TMDCs have shown significant promise, the emerging family of 2D metal monochalcogenides (MMCs), particularly from groups III-VI and IV-VI, has recently garnered intense scrutiny due to their distinctive electronic symmetries and carrier transport mechanisms that often surpass their dichalcogenide counterparts [5], [6].

MMCs such as GaS, GaSe, InSe, and GeSe represent a behaviourally diverse library of layered semiconductors held together by weak van der Waals (vdW) forces. Unlike the well-documented indirect-to-direct bandgap transition observed in bulk TMDCs upon thinning to a monolayer, many MMCs-most notably those based on Gallium-exhibit a unique direct-to-indirect transition as layer numbers decrease [7]. This property, combined with their high surface-to-volume ratios and tunable band edges, makes them exceptionally sensitive to environmental stimuli and light-matter interactions, positioning them as ideal candidates for multispectral photodetection across the ultraviolet (UV), visible, and near-infrared (NIR) spectra [8].

Within the MMC family, Gallium-based systems (GaX, where X: S, Se) have emerged as the primary focus of contemporary "Advances" in the field for several strategic reasons. Gallium Selenide (GaSe) is one of the few stable p-type 2D semiconductors available, a rarity in a landscape dominated by n-type materials, which facilitates the design of efficient p–n junctions without the complexities of extrinsic doping [9], [10]. Simultaneously, Gallium Sulfide (GaS) possesses a wide bandgap (~3.0 eV), making it inherently solar-blind and highly effective for UV sensing [11]. Recent researches has pushed these materials beyond the laboratory stage, with significant breakthroughs in controllable chemical vapor deposition (CVD) of vertical nanoflower morphologies and molecular beam epitaxy (MBE) on graphene platforms for in situ band engineering [12], [13].

The current research frontier is now shifting from fundamental material synthesis to complex heterojunction engineering. By pairing p-GaSe with n-type oxides or TMDCs, researchers have achieved self-powered, high-gain photodetectors that leverage interfacial photogating and built-in electric fields to reach record-breaking responsivities and detectivities [14]. Furthermore, the move toward flexible and wearable electronics has driven the development of printed GaS-based sensors and bendable vdW stacks, although stability under ambient conditions remains a critical engineering challenge [13], [15].

This review aims to provide a comprehensive synthesis of these recent developments. We begin by detailing the fundamental sensing mechanisms and figures-of-merit that define photodetector performance. Subsequently, we explore the evolution of synthesis strategies from top-down exfoliation to advanced bottom-up techniques. A comparative analysis will highlight the unique bandgap physics of MMCs versus TMDCs, followed by an in-depth discussion on the state-of-the-art in Ga-based heterojunctions and their integration into the next generation of flexible, self-powered optoelectronic devices.

II. SENSING MECHANISMS AND FIGURES-OF-MERIT

There are three dominant sensing mechanisms in photodetectors based on 2D layered semiconductor, namely, photoconductive effect, photogating effect, and photovoltaic effect [16]. Each of these mechanism is described in brief in the following section. The fundamental electronic processes governing the transformation of optical energy into measurable photocurrent-specifically through carrier generation, trap-mediated gating, and junction-induced separation-are schematically illustrated in **Fig. 1**.

A. Photoconductive Effect

The photoconductive effect is a phenomenon observed in photodetectors, where the absorption of light causes an increase in the conductivity of the semiconductor channel. Photoconductors, based on this effect, consist of a semiconducting channel layer with two ohmic contacts acting as source and drain electrodes. When light of sufficient energy is incident on the channel area, electron-hole pairs are generated and separated by the applied bias between the source and drain electrodes. This results in a net increase in channel current. In the case of an n-type semiconductor, electrons, which are the majority carriers, are rapidly transported from the source to drain via the channel. This process is completed in a very short time, which is referred to as the electron transit time, denoted by $\tau_{transit}$. However, minority carriers, which are the holes in this case, travel much more slowly towards the respective electrode. During the lifespan of holes, denoted by $\tau_{lifetime}$, the other electrode provides extra electrons to maintain charge neutrality, and these electrons circulate across the channel several times. The gain, G, of a photoconductor is determined by the ratio of hole lifetime to electron transit time, i.e., $G = \frac{\tau_{lifetime}}{\tau_{transit}}$. A photoconductor exhibits a gain that is greater than unity. For a higher gain, the electron transit time should be shorter, and the hole lifetime should be longer. However, achieving higher gain comes at the cost of a slower response speed of the detector. Therefore, a trade-off must be maintained between the response speed and gain to achieve standard performance [14], [17],

B. Photogating Effect

The photogating effect is a specific case of the photoconductive effect, which is observed in materials with a high density of defects that trap one type of photogenerated carriers.

When these materials are illuminated, electron-hole pairs are generated in the active medium, which then move towards their respective electrodes under an external bias. In materials with a high number of defect sites, one type of charge carrier (for example, holes) can become trapped at these sites, which then function as local gates. These local gates provide an additional gate voltage that can reduce the overall resistance of the channel.

The trapped carriers can then recirculate multiple times, leading to high gain. Low-dimensional materials with a high surface-to-volume ratio, such as 2D layered materials, are especially prone to the photogating effect. However, despite having a larger gain than photoconductors, photodetectors with photogating effect often exhibit a slower response speed. This is because the trapped carriers have a limited lifespan, and the recirculation process can take longer to produce a significant photocurrent. It is worth noting that in some cases, both the photogating effect and the photoconductive effect can contribute to the photocurrent in the same device, leading to more complex behaviour. Nevertheless, the photogating effect remains an important phenomenon for the design and optimization of photodetectors and other optoelectronic devices that rely on the generation and detection of light-induced carriers [14], [17].

ISSN: 2321-9653; IC Value: 45.98; SJ Impact Factor: 7.538
Volume 14 Issue II Feb 2026- Available at www.ijraset.com

C. Photovoltaic Effect

The photovoltaic effect is observed in devices with a built-in electric field that separates photogenerated charge carriers under no bias conditions. This electric field is typically developed at a junction where there is a substantial difference between the work function values of the constituent materials. Photodetectors that operate via the photovoltaic effect are referred to as photodiodes, and some examples include p-n photodiodes, p-i-n photodiodes, and avalanche diodes. Under dark conditions, the current-voltage characteristic of a photodiode exhibits a rectifying nature, while under illumination, it can be operated in two modes: photovoltaic mode (operated at zero bias) and photoconductive mode (operated under reverse-bias). In photovoltaic mode, the built-in electric field sweeps away the photogenerated electron-hole pairs in opposite directions, generating a significant photocurrent that is collected in the respective electrodes. In contrast, in photoconductive mode, the external electric field adds up to the built-in electric field, thereby increasing the carrier collection efficiency and response speed. Typically, photodiodes have a maximum gain of unity, which is substantially lower than photodetectors that operate via the photogating effect or the photoconductive effect. Although photodiodes are useful for many applications, they have limited gain, which restricts their use in low-light conditions. In contrast, photodetectors that operate via the photogating effect or the photoconductive effect can have much higher gain, but they also tend to have slower response times. The choice of photodetector depends on specific application requirements, such as sensitivity, response time, and dynamic range [18].

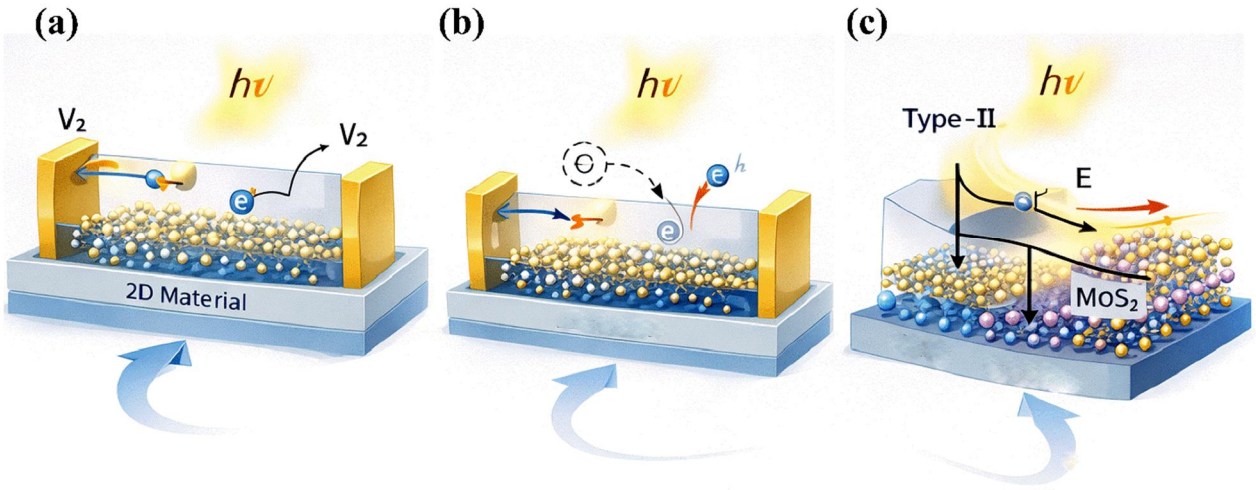

Fig. 1: Schematic representation of the primary sensing mechanisms in 2D-based photodetectors: (a) the photoconductive effect involving bias-driven carrier transport; (b) the photogating effect driven by defect-assisted carrier trapping; and (c) the photovoltaic effect facilitated by built-in electric fields at a heterojunction interface.

D. Figures-of-merit of a photodetector

Photodetectors are assessed based on specific parameters referred to as performance parameters or figures of merit. These parameters are crucial in determining the effectiveness of the photodetector. Some of the key figures of merit include dark current, illumination current, photocurrent, photo-to-dark current ratio, photoresponsivity, specific detectivity, noise equivalent power, external quantum efficiency, and response time. Each of these parameters plays a significant role in determining the overall performance of the photodetector [16], [19].

(i) Dark current (I_d)

Dark current (I_d) is the term used to describe the current flowing through a photodetector when there is no light present. A desirable characteristic of a high-quality photodetector is to have a low level of dark current.

(ii) Illumination current (I_λ)

The illumination current (I_λ) refers to the total current flowing through the photodetector when it is exposed to light of a specific wavelength (λ). A high value of illumination current is desirable for a photodetector to be considered effective.

(iii) Photocurrent (I_{ph})

The difference between the illumination current (I_λ) and the dark current (I_d) is known as the photocurrent (I_{ph}) of a photodetector. Mathematically, it is expressed as:

$$I_{ph} = I_\lambda - I_d \tag{1.1}$$

A higher value of photocurrent indicates better performance for a photodetector.

(iv) Photo-to-dark current ratio (PDCR)

The ratio of photocurrent (I_{ph}) to the dark current (I_d) is known as the photo-to-dark current ratio (PDCR) of the photodetector. It is given by:

$$PDCR = \frac{I_{ph}}{I_d} = \frac{I_\lambda - I_d}{I_d} \tag{1.2}$$

The performance of a photodetector is considered better when it exhibits higher values of PDCR.

(v) Photoresponsivity (R_λ)

Photoresponsivity (R_λ) is the measure of efficiency of a photodetector in responding to an incident photon and it is defined as the amount of photo generated current (I_{ph}) per unit power incident on the effective device area. It is expressed in the unit of $A\,W^{-1}$. Mathematically,

$$R_\lambda = \frac{I_{ph}}{P_\lambda A} = \frac{I_\lambda - I_d}{P_\lambda A} \tag{1.3}$$

Where, P_λ is the power density of the incident light and A is the effective device area. Photoresponsivity (R_λ) is a very crucial parameter of a photodetector in investigating the spectral response and wavelength range selection. Higher values of photoresponsivity indicates a better performance of a photodetector.

(vi) Noise equivalent power (NEP)

The term "noise equivalent power" (NEP) refers to the minimum power detectable per square root bandwidth of a photodetector. In unit of $W/\sqrt{\text{Hz}}$, NEP can be expressed as[15]:

$$NEP = \frac{i_{noise}}{R_\lambda} \tag{1.4}$$

Where, i_{noise} expresses the noise current, defined mathematically at a detection bandwidth B as:

$$i_{noise} = \sqrt{i_{shot}^2 + i_{thermal}^2 + i_{trap}^2}$$
$$= \sqrt{2eI_dB + \frac{4k_BT}{R_{sh}}B + i_{trap}^2} \tag{1.5}$$

Where, k_B is the Boltzmann's constant, R_{sh} is the shunt resistance of the device. In equation (1.5), the first term in the square root represents the shot noise, the second term denotes the thermal noise, and the third term is the noise current component, originating from the sub-bandgap trap states in the photodetector.

(vii) Specific detectivity (D^*)

The ability to detect and distinguish weak optical signals from the noise is represented by specific detectivity *(D^*)*. Mathematically, D^* is expressed by[20]:

$$D^* = \frac{\sqrt{A\Delta f}}{NEP} \tag{1.6}$$

Where, Δf the electrical bandwidth measured in Hz.

In cases where the shot noise resulting from the dark current is the major source of noise in a photodetector, D* can be expressed by the following equation[21]:

$$D^* = \frac{R_\lambda \sqrt{A}}{\sqrt{2eI_d}} \tag{1.7}$$

Where, e is the charge of an electron. In general, equation (1.7) is used to calculate the specific detectivity of UV-vis photodetectors [22][9], [10], [23]. D^* is expressed in the units of Jones, whereby 1 Jones =1 cm$-\sqrt{\text{Hz}}\,W^{-1}$. The higher values of specific detectivity indicate a better performance of a photodetector.

(viii) External quantum efficiency (EQE)

External quantum efficiency (EQE) gives a measure of the number of electron-hole pairs created by one absorbed photon. It is expressed mathematically as:

$$EQE = \frac{hcR_\lambda}{e\lambda} \tag{1.8}$$

Where, h is the Plank's constant.

EQE is expressed in percentage (%). A high value of EQE is desired in a good photodetector.

(ix) Response time (τ)

Response time (τ) is a crucial performance parameter for a photodetector. The response time of a photodetector is the time it takes for the output to change in response to a change in the input signal. The response time is found on both the rising (rise time) and falling (fall time) edge of the signal. Rise time is defined as the time taken by the photocurrent to enhance from 10% to 90% of its maximum value and in contrast decay time is defined as the time taken by the photocurrent to fall from 90% to 10% of its maximum value.

The trap-assisted photocurrent in response to the laser light illumination on a photodetector follows a bi-exponential equation:

$$I(t) = I_0 + A_1 e^{-\frac{(t-t_0)}{\tau_1}} + A_2 e^{-\frac{(t-t_0)}{\tau_2}} \tag{1.9}$$

Where, I_0 is the current at steady state; A_1, A_2 are the scaling factors; τ_1, τ_2 are relaxation time constants; t_0 and t have the unit of time. Both rise and decay times have two components, namely, fast and slow components. The fast component is attributed to the sudden enhancement in carrier concentration upon illumination. In contrast, the slow component comes from the defects influenced charge carrier trapping/de-trapping mechanism [24], [25].

(x) Gain (G)

The gain of a photodetector represents the number of charge carriers detected by the photodetector for each incident photon. It is expressed by the following equation:

$$G = \frac{I_{ph}/e}{\eta P_{in}/h\nu} = R_\lambda \frac{hc}{\eta e\lambda} \tag{1.10}$$

Where, η is the quantum efficiency of the device and P_{in} is the incident optical power.

(xi) Linear dynamic range (LDR)

The linear dynamic range (LDR) of a photodetector refers to the range of input optical power levels that produce a linear response in the output electrical signal. This range can be determined mathematically using the following formula [26]:

$$LDR = 10 \log\left(\frac{P_{sat}R}{\sqrt{2eI_dB}}\right) \tag{1.11}$$

Where, P_{sat} refers to the optical power level at which the photocurrent ceases to exhibit linear characteristics and becomes saturated with an increase in optical illumination.

III. SYNTHESIS AND ASSEMBLY METHODS FOR METAL MONOCHALCOGENIDES

The reliable production of individual MMCs is essential for their practical application in the fields of electronics and optoelectronics. Generally, the synthesis methods for MMCs can be divided into two categories: top-down and bottom-up approaches. These methods encompass techniques such as mechanical or chemical exfoliation [27] - [28], vapor deposition [29], solvothermal method [30], pulsed laser deposition, and more. In the following section, we will provide a brief examination of these synthesis methods for MMCs. A schematic of MMCs synthesis/assembly routes has been illustrated in Fig. 2.

A. Top-down methods

The bonding between individual layers in TDLMs (Two-Dimensional Layered Materials) is primarily maintained through weak van der Waals forces, allowing for easy separation of these layers. Mechanical exfoliation, chemical exfoliation, and intercalation of molecules/atoms in the liquid phase are the most commonly used methods to obtain single or few-layer TDLMs.

1) Mechanical Exfoliation

Mechanical exfoliation is a straightforward method for obtaining individual layers of 2D materials from a bulk material by applying mechanical force. The pioneering work of Geim and Novoselov[1] introduced this technique when they successfully derived graphene from graphite using a micromechanical cleavage approach. In the typical process of micromechanical exfoliation, thin-layered crystals are initially scraped off from the bulk crystal using adhesive Scotch tape. Subsequently, the freshly cleaved thin crystals on the Scotch tape are brought into contact with the desired substrate and rubbed to further separate them. Once the Scotch tape is removed, single-layer and multilayer nanosheets remain on the substrate. It is widely recognized that the mechanical exfoliation technique yields single or few-layer TDLMs with excellent quality, characterized by clean and micrometer-sized flakes on various substrates. These flakes are highly suitable for fundamental research purposes and for demonstrating high-performance devices [5], [31].

To date, several MMCs, such as GaS, GaSe, InSe, GaTe, and In_2Se_3, have been synthesized using mechanical exfoliation methods. For instance, Tamalampudi *et al.*[32] designed highly efficient photodetectors based on mechanically exfoliated few-layered InSe flakes. These photodetectors were fabricated on both rigid SiO_2/Si substrates and flexible polyethylene terephthalate (PET) films. The devices exhibited broadband photoresponse, covering the visible to near-infrared region (450−785 nm), with high photoresponsivities of up to 12.3 AW^{-1} at 450 nm (on SiO_2/Si) and 3.9 AW^{-1} at 633 nm (on PET). Hu *et al.*[33] also reported their results on a mechanically exfoliated GaSe-based photodetector, which demonstrated a remarkable photoresponsivity of 2.8 AW^{-1} and an external quantum efficiency (EQE) of 1367% at 254 nm. Additionally, they designed another photodetector based on GaS nanosheet, produced via the same mechanical exfoliation technique[11]. The GaS nanosheet-based photodetector gave a photoresponsivity of 4.2 AW^{-1} on a rigid substrate and a considerably higher value of 19.2 AW^{-1} of the same on a flexible substrate. Subsequently, Yang *et al.*[34] reported even a higher photoresponsivity of 64.43 AW^{-1} and an EQE value of 12621%, from their mechanically exfoliated layered GaS nanosheets, when exposed to an ammonia environment. Thus, mechanically exfoliated MMCs have a great potential in the development of high-performance photodetectors. However, it is important to note that despite the successful synthesis of MMCs through mechanical exfoliation, this method is not suitable for large-scale production due to the lack of control over the morphology and yield of the flakes.

2) Liquid Phase Exfoliation

Alternatively, liquid phase exfoliation (LPE) has emerged as a promising method for the synthesis of MMCs in large scale. It involves dispersing bulk MMC materials in a suitable liquid solvent and subjecting them to various energy inputs such as ultrasonication or shear mixing. These energy inputs effectively exfoliate the bulk material into few-layered nanosheets or even single-layer flakes. For instance, researchers have successfully utilized this technique to exfoliate MMCs such as GaS, GaSe, InSe, GaTe, and In_2Se_3. By dispersing the bulk MMCs in solvents such as N-methyl-2-pyrrolidone (NMP), isopropyl alcohol (IPA), or water, and applying ultrasound or mechanical agitation, nanosheets or flakes of the desired MMCs can be obtained [35]. Chan *et al.* [36] used shear exfoliation method to produce dispersed GaSe nanoflakes of different shapes and sizes. By subjecting the layered GaSe crystal to shear mixing for 3 hours at 8000 rpm, they successfully achieved the exfoliated nanosheets.

Layer number controllability and large-area uniformity are crucial prerequisites for the practical application of electronic and optoelectronic devices. While top-down exfoliation methods fall short in meeting these requirements, bottom-up methods have emerged as promising approaches for the large-scale production of single or few-layer MMCs. In the subsequent section, we will delve into these methods, shedding light on their effectiveness and potential.

B. Bottom-up methods

The bottom-up methods encompass a range of techniques such as physical vapor deposition (PVD), chemical vapor deposition (CVD), and pulsed laser deposition (PLD). These techniques have demonstrated their ability to produce pristine, wafer-scale, and high-quality 2D layered materials, featuring customizable thickness, lateral size, and well-defined geometries, while ensuring excellent repeatability. Consequently, the bottom-up approach yields 2D layered materials that are highly suitable for cutting-edge electronic and optoelectronic applications.

1) The physical vapor deposition (PVD) method

PVD is a process where a material is vaporized from a solid source and then condensed onto a substrate to form a thin film. The vaporization is typically achieved through physical methods such as evaporation or sputtering. Evaporation involves heating the source material to a high temperature, causing it to sublimate and form a vapor.

Sputtering, on the other hand, uses energetic particles (usually ions) to dislodge atoms from the source material and create a vapor. The vapor then travels to the substrate and condenses, forming a thin film. Lei *et al.*[29] successfully utilized the PVD method to grow large-area few-layer GaSe crystals directly on insulating substrates.

The results obtained were similar to those of mechanically exfoliated samples. In their photocurrent measurement, they observed a clear electrical photoresponse and also achieved a desired low dark current. PVD method was also used by Zhou *et al.*[37] to obtain α-In_2Se_3 monolayer on SiO_2/Si substrate. By varying the growth time, the atomic layers of α-In_2Se_3 could be produced with different thicknesses and geometries. The procedure was replicated to achieve the controlled synthesis of ultrathin GaSe nanoplates on a flexible mica substrate[38]. These nanoplates exhibited usual p-type behavior and showed strong sensitivity to light. Moreover, when the GaSe-based devices, fabricated on flexible mica substrates, were subjected to repeated bending at different radii, they maintained efficient photoresponse.

2) The chemical vapor deposition (CVD) method

The CVD process involves vapor-phase precursors reacting chemically at the surface of the substrate to create a coating that is not easily vaporized. This process consists of two primary components: (i) the movement of gas-phase materials to the reaction area and their subsequent reactions, and (ii) the formation of a film on the substrate.

Gas-phase materials are transported through a combination of convection caused by pressure differences and the diffusion of gaseous reactants towards the substrate. The deposition takes place when the reactant adheres to the substrate through surface chemical reactions. In numerous studies, the production of large-scale TDLMs through the CVD method has been showcased, with a particular emphasis on MoS_2[39], [40].

To date, only a limited number of reports have focused on the synthesis of monolayer or few-layer MMCs using the CVD method. Among these reports, Li *et al.*[41] presented a notable approach for synthesizing GaSe. In their study, they utilized a molar ratio of approximately 50:1 of GaSe and Ga_2Se_3 as the raw materials.

By adjusting the growth factors such as duration, temperature, growth area, and argon carrier gas flow rate, they obtained a control over the size, density, shape, thickness, and uniformity of 2D GaSe crystals. Chang *et al.*[42] presented a significant advancement in the synthesis of large-area InSe monolayers via CVD method. They took In_2O_3 powder and Se powder as precursors. For the carrier gas, a specific mixture of H_2 and Ar gas were used. The resulting triangular-shaped InSe monolayers possessed perfect crystallinity and an impressive lateral size of up to 250 μm.

3) The pulsed laser Deposition (PLD) Method

Pulsed Laser Deposition (PLD) is a thin film deposition technique that involves using a high-energy laser to ablate a target material and deposit it onto a substrate to create thin films. In the PLD process, a laser beam is focused on the target material, which is typically in the form of a solid.

The laser ablates the target material, causing it to vaporize and form a plasma plume. The plume expands and deposits onto the substrate, where it cools and solidifies, forming a thin film[43]. Recently, Mahjouri-Samani *et al.*[44] presented a study detailing the fabrication of GaSe nanosheets using the PLD technique. The group achieved this by performing a stoichiometric transfer of laser-vaporized material from bulk GaSe targets.

By employing low-intensity laser pulses, they successfully produced individual triangular GaSe nanosheets comprising $1-3$ layers, with an average domain size of around 200 nm. Increasing the laser pulses up to 100 led to the formation of GaSe nanosheet networks.

The research findings indicated that these nanosheet networks exhibited p-type behaviour, displaying high mobilities of up to 0.1 cm^2/Vs. To address the need for improved nucleation density and average size, the researchers combined the PLD method with a vapor transport growth (VTG) system to obtain ~100 μm large and crystalline 2D GaSe and $MoSe_2$ nanosheets. This was achieved by accurately controlling the mass and location of the source materials. The procedure involved depositing nanoparticles onto a substrate using PLD at room temperature, followed by placing a receiver substrate on top of the source substrate to create a confined VTG system. This combined PLD-VTG technique introduced a novel approach for controlled growth of metal chalcogenides over extensive areas, ensuring a specific number of layers at predetermined patterned growth locations. This development holds significant promise for applications in photodetection.

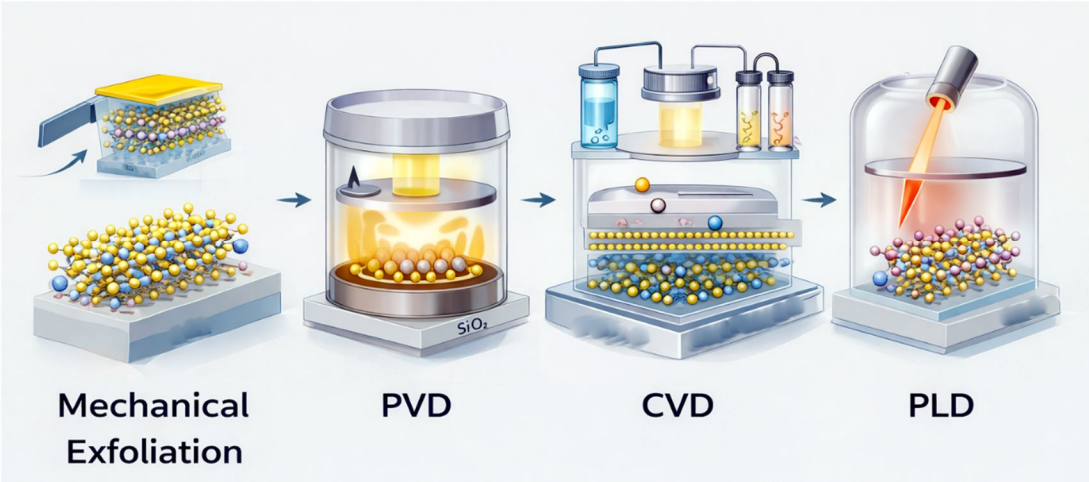

Fig. 2: Schematic of MMCs synthesis/assembly routes: mechanical exfoliation, PVD, CVD, and PLD—showing material transfer/growth onto SiO_2/Si substrates and the quality-scalability trade-off across methods.

IV. FUNDAMENTAL PHYSICS AND ULTRAFAST INTERFACIAL DYNAMICS

The exceptional performance of Gallium-based Metal Monochalcogenide (MMC) photodetectors is rooted in their ultrafast interfacial dynamics, which govern the efficiency of charge separation, carrier extraction, and recombination suppression. Unlike traditional three-dimensional (3D) semiconductors, where charge transfer is limited by bulk recombination and trap-assisted losses, two-dimensional (2D) van der Waals (vdW) heterojunctions offer atomically sharp interfaces with minimal defect densities and tunable band alignments [45], [46]. This section provides a critical synthesis of the latest experimental and computational research, contrasting Transient Absorption Spectroscopy (TAS) measurements with Non-Adiabatic Molecular Dynamics (NAMD) and Density Functional Theory (DFT) predictions to establish a quantitative framework for understanding interfacial charge transfer in Ga-based systems.

A. Interfacial Charge Transfer: Time Constants and Mechanistic Pathways

1) Computational Predictions: NAMD and DFT Insights

The efficiency of a vdW heterojunction depends critically on how rapidly photogenerated electron-hole (e-h) pairs separate across the interface before recombination. Recent Non-Adiabatic Molecular Dynamics (NAMD) simulations have provided the first quantitative predictions for Gallium-based heterostructures, revealing transfer time constants that were previously unresolved experimentally.

Yan et al. (2025) performed NAMD calculations on a prototype GaSe/GaTe heterobilayer and reported that:

- Electron transfer occurs in the range of 97–390 fs depending on the stacking registry (AA′ vs. A′A).
- Hole transfer is significantly faster, ranging from 40–126 fs.
- Most importantly, certain stacking configurations (specifically AA′ and A′A) can dramatically prolong carrier lifetimes to 213 nanoseconds, representing a factor of ~10^4 increase over typical TMDC recombination times [46].

These predictions are grounded in the observation that Ga-based MMCs exhibit weak nonadiabatic (NA) coupling between electronic states and dominant low-frequency phonon modes that suppress electron-hole recombination. This is in stark contrast to TMDC-only systems, where strong NA coupling typically drives rapid recombination on picosecond timescales.

2) DFT Band Alignment Studies:

Several first-principles DFT studies have characterized the electronic structure of GaSe- and GaS-based heterojunctions:

- Kumar et al. analyzed the MoS_2/GaS heterostructure using DFT and confirmed a Type-II band alignment with a predicted direct bandgap favourable for efficient charge separation [47].
- Ma et al. investigated GaSe/ZnS using HSE06-corrected DFT and reported high carrier mobilities (electrons: ~10^3 cm^2/Vs) and strong optical absorption in the visible range, though explicit transfer time constants were not computed [48].
- Liu et al. studied GaS/PtSSe under biaxial strain and external electric fields, demonstrating that band alignment and transfer efficiency can be actively tuned by mechanical or electrical stimuli [49].

While NAMD provides the "forward prediction" of transfer rates, DFT studies establish the electronic landscape (band offsets, work functions, and density of states) that enables these ultrafast processes. The consensus from recent computational work is that Ga-based MMCs possess intrinsic electronic structures that favour both rapid initial separation and prolonged carrier lifetimes when properly engineered [48], [49], [50] .

B. Experimental TAS Measurements: The Current State

Despite the wealth of computational predictions, experimental verification of sub-100 fs transfer times in GaSe/MoS_2 and GaSe/WS_2 heterojunctions remains limited. The primary challenge is the sub-picosecond resolution required to capture the initial charge separation event, which demands femtosecond pump-probe setups with sub-20 fs pulse durations.

Li et al. fabricated vertical GaSe/MoS_2 heterojunctions and characterized them using steady-state photoluminescence (PL) and current-voltage (I-V) measurements. While they reported high responsivity (42.6 A/W at 300 nm) and detectivity (8.17×10^{12} Jones), no time-resolved TAS data were provided to directly measure the charge transfer rate [49]. Soni et al. performed femtosecond TAS on a WS_2/Ruddlesden-Popper perovskite hybrid heterostructure and observed hole transfer within 260 fs and interlayer exciton lifetimes of 728 ps [51]. Although this is not a Ga-MMC system, it demonstrates that fs-resolution TAS is now routinely achievable and sets a benchmark for future Ga-based studies. Rafizadeh et al. used TAS to study $MoSe_2$/WS_2 and identified coexisting Type-I and Type-II interfaces depending on layer thickness, with evidence of charge transfer in the Type-II regime, though explicit time constants were not reported in the abstract [52]. A comprehensive multi-scale overview of the unique bandgap evolution, atomic tetralayer structure, and superior optoelectronic performance metrics of Ga-based MMCs is summarized in Fig. 3.

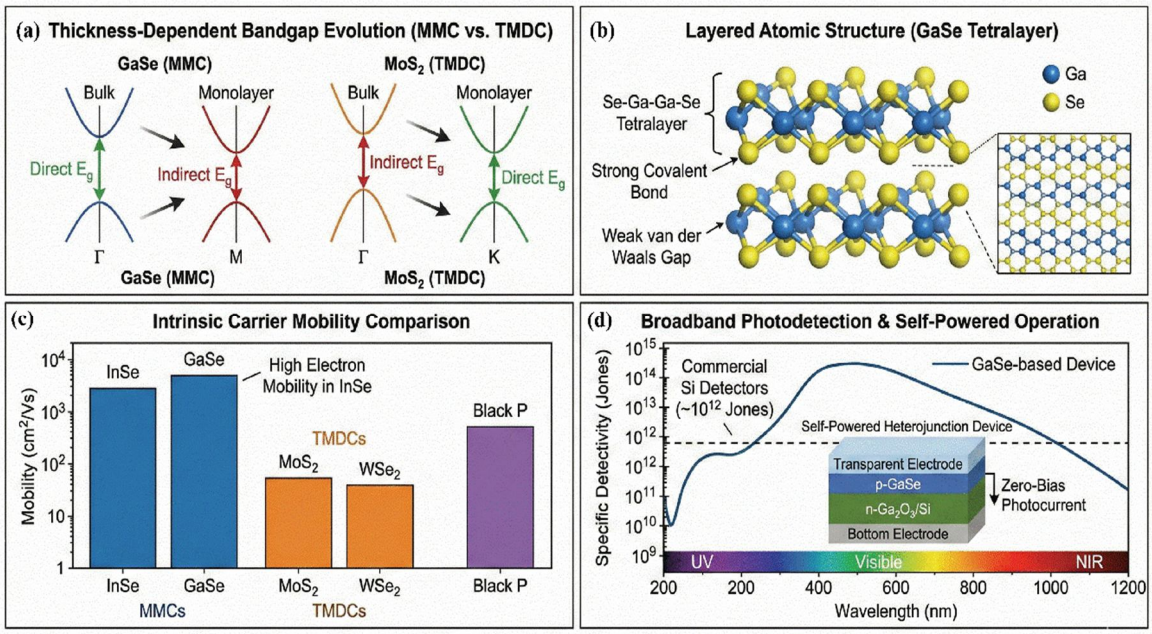

Fig. 3: (a) Contrasting bandgap transitions in MMCs and TMDCs upon thinning. (b) Atomic structure of layered GaSe. (c) Superior carrier mobility of MMCs compared to other 2D materials. (d) High specific detectivity across a broad spectrum and schematic of a self-powered MMC-based heterojunction photodiode.

V. COMPARATIVE ANALYSIS: GA-MMCS VS. TMDC-ONLY HETEROSTRUCTURES

The central question addressed in this section is: How do Gallium-based MMCs (GaSe, GaS) compare to traditional TMDC-only heterojunctions (MoS_2/WS_2, $MoSe_2$/WSe_2) in terms of charge transfer speed, carrier lifetime, and "stacking tunability"? By synthesizing recent breakthroughs in ultrafast spectroscopy and ab initio simulations, we demonstrate that Ga-MMCs offer a unique wide dynamic range of carrier dynamics—from sub-100 femtosecond (fs) separation to hundred-nanosecond (ns) recombination times—making them superior platforms for simultaneous high-speed and high-gain photodetection.

To appreciate the unique advantages of Ga-based MMCs, we must compare their dynamics to the well-studied TMDC-only systems.

A. TMDC-Only Dynamics

Recent many-body calculations (GW + Bethe-Salpeter Equation + exciton-phonon coupling) for MoS_2 and WS_2 monolayers **predict exciton relaxation times as short as:**

- **≈ 67 fs for MoS_2**
- **≈ 15 fs for WS_2 at 300 K [53].**

These ultrafast relaxation rates are driven by strong exciton-phonon coupling, which opens new "phonon-assisted" transfer channels that bypass traditional energy barriers. Time-dependent DFT studies of MoS_2/WS_2 bilayers show that stacking can modulate interlayer charge transfer from ~100 fs to ~1 ps, but the overall timescale remains firmly in the sub-picosecond regime [53].

B. Ga-MMC Advantages

(i) Wider Dynamic Range: While TMDCs are confined to fs–ps transfer and recombination, Ga-MMCs can achieve:

- Fast separation: 40–390 fs (comparable to TMDCs).
- Prolonged lifetimes: Up to 213 ns (orders of magnitude longer than TMDCs) [50].

(ii) Stacking Tunability: In TMDCs, stacking primarily affects the transfer speed within a narrow window. In Ga-MMCs, stacking can toggle between high-speed/low-gain (fast recombination) and moderate-speed/high-gain (long lifetimes), providing a superior "physics-to-engineering" lever.

(iii) Recombination Suppression: The weak NA coupling in Ga-MMCs means that even after rapid initial separation, carriers remain spatially separated for extended periods, enabling photocurrent gains (G) exceeding 10^3 in optimized devices [45], [50].

To explicitly quantify these temporal advantages, a direct comparison of electron/hole transfer times and overall carrier lifetimes across various 2D systems is summarized in **Table 1.**

TABLE 1
COMPARATIVE CHARGE TRANSFER DYNAMICS

System	Electron Transfer	Hole Transfer	Carrier Lifetime	Method	Reference
GaSe/GaTe (AA′ stacking)	97 fs	40 fs	213 ns	NAMD	Yan et al. [50]
GaSe/GaTe (A′A stacking)	390 fs	126 fs	~ 12 ns	NAMD	Yan et al. [50]
MoS_2/WS_2	~ 100 fs–1 ps	Not specified	~ 1 ps	TD-DFT	(Comparative) [54]
WS_2/perovskite	Not specified	260 fs	728 ps	TAS	Soni et al. [54]
MoS_2 monolayer	N/A	N/A	≈ 67 fs	GW+BSE	(Theory) [53]

C. The Role of Exciton-Phonon Coupling and Non-Adiabatic Mechanisms

Exciton-phonon coupling plays contrasting roles depending on the material system and the dominant phonon modes. Many-body calculations reveal that strong exciton-phonon interactions in TMDCs enable ultrafast intralayer-to-interlayer exciton conversion by creating new relaxation pathways. Specifically:

- High-frequency optical phonons (~200–400 cm^{-1}) couple strongly to excitons, enabling sub-50 fs transitions that are not possible in rigid-lattice models.
- This phonon-mediated transfer is so fast that it sets a thermodynamic limit on the maximum achievable carrier extraction efficiency [53].

D. Stacking Modulation: Engineering the Ultimate Photodetector

The most transformative insight from current research is that atomic-scale stacking can be used as a "dial" to tune photodetector performance.

(i) AA′ Stacking (High-Gain Mode): Maximizes the suppression of NA coupling, leading to the longest carrier lifetimes (213 ns in GaSe/GaTe) [49]. Ideal for low-light detection where high gain is critical.

(ii) AB Stacking (High-Speed Mode): Stronger interlayer electronic coupling facilitates faster transfer (~100 fs) but also faster recombination (~1 ps). Ideal for high-bandwidth communication where speed trumps gain.

While TMDC-only stacks show some stacking sensitivity (100 fs vs. 1 ps), the magnitude of tunability in Ga-MMCs is unprecedented: a factor of ~10^4 in carrier lifetime by simply changing the atomic registry [50]. This makes Ga-based systems uniquely suited for reconfigurable optoelectronics where a single material platform can be optimized for different applications by post-fabrication stacking control.

VI. GA-BASED MMCS: GAX AND GAX_2 (X: S/SE), HETEROJUNCTIONS, PHOTODETECTORS, AND THEIR CURRENT STATUS

The Ga-based MMCs which have attracted a huge attention of the material researchers are GaS and GaSe. These III-VI metal monochalcogenides have almost similar crystal structures, which closely resemble to that of graphene and TMDCs. These MMCs exhibit a hexagonal structure characterized by a honeycomb arrangement. Each layer of the structure is composed of tightly bonded atoms represented by X-M-M-X, where M denotes the metal atom and X represents the chalcogen atom. Each monolayer of GaSe and GaS is around 0.9 nm and 0.7 nm thick, respectively. The layers in these MMCs are stacked on top of each other and are held together by weak van der Waals forces. The distinct stacking arrangements of the layers give rise to four primary polytypes, specifically β, γ, δ, and ε [29], [34]. Unlike TMDCs, which undergo a transition from an indirect to a direct bandgap in the monolayer limit, the behaviour of the bandgap in GaS and GaSe differs when the material is thinned down to a monolayer from its bulk form. GaSe has direct bandgap energy of ~2 eV in bulk form and an indirect bandgap of ~3.5 eV in the monolayer form[7]. On the other hand, GaS has a direct band gap of ~3.05 eV in its bulk form and an indirect bandgap of ~2.59 eV in the monolayer form[11]. As the thickness of these materials decreases, there is a notable increase in the bandgap of these materials.

The pioneering work on GaS nanosheet-based photodetectors was conducted by Hu *et al* [11]. Their study involved the fabrication of GaS-based devices on both rigid and flexible substrates. These photodetectors exhibited remarkable photoresponsivities, reaching up to 19.2 AW^{-1} in the ultraviolet range, accompanied by exceptional external quantum yields of up to 9374% at 254 nm. Notably, these values surpass the performance of pristine graphene photodetectors, which typically demonstrate photoresponsivities of 10^{-3} AW^{-1} and external quantum yields ranging from 6−16%. A two-terminal photodetector based on few-layer GaS was developed by Yang *et al.*[34] Their study revealed a rapid and consistent response from the device. Interestingly, the photodetector displayed distinct photoresponse when exposed to different gas environments. Notably, a significantly higher photoresponse of 64.43 AW^{-1} and an EQE of 12621% were achieved when the device was exposed to ammonia (NH_3), as compared to air or oxygen (O_2) environments. The researchers also conducted theoretical investigations, which indicated that the variation in photo-responses is attributed to the charge transfer occurring between the adsorbed gas molecules and the photodetector. GaSe nanosheets-based photodetectors exhibit exceptional photoresponse characteristics across both the ultraviolet (UV) and visible regions. The remarkable photoresponse performance can be attributed to the highly resistive layered structure of GaSe, coupled with the low hall mobility of its charge carriers. These factors contribute to a significantly low dark current in GaSe-based photodetectors, which is of paramount importance for effective photodetection applications[55]. Ultrathin GaSe nanosheets were obtained by Huang *et al.* [5] through the micromechanical cleavage technique, utilizing commercially available bulk GaSe crystals. These nanosheets were then transferred onto SiO_2/Si substrates, where interdigitated electrodes (IDE) were employed to fabricate field-effect transistors (FETs). The researchers observed a linear increase in the photocurrent relative to the incident power density in their devices. Notably, a maximum photoresponsivity of 2.2 AW^{-1} was achieved at a wavelength of 520 nm, and the I_{photo}/I_{dark} ratio reached approximately 10^3, indicating a significant differentiation between the photocurrent and dark current levels. Sorifi *et al.*[56] fabricated a metal-semiconductor-metal (MSM) photodetector based on multilayered GaSe, utilizing Ti/Au as the metal contacts. When illuminated with a 380 nm laser, the photodetector demonstrated a significant increase in photocurrent. At room temperature and a power density of 0.35 mW/cm^2, the device exhibited a photoresponsivity of 2.6 AW^{-1}, an EQE value of 850%, and a detectivity of 1.0×10^{12} Jones. The experimental results indicated a high photoresponse in both the ultraviolet (UV) and visible regions. Furthermore, the thermal stability of the GaSe-based photodetector was examined across various temperatures, ranging from room temperature to 120 °C. Remarkably, even at 120 °C, the photodetector remained thermally stable and achieved a maximum photoresponsivity of 4.5 AW^{-1}.

Ga-based MMCs also play significant roles in fabricating heterojunction photodetectors. Wang *et al.* developed a GaSe/Ga_2O_3 vertical heterojunction by exfoliating GaSe flakes onto a β- Ga_2O_3 substrate. The resulting van der Waals heterojunction device exhibited negligible dark current and showcased outstanding detectivity, sensitivity, and speed. Notably, it achieved a maximum photoresponsivity of 51.9 AW^{-1} and a specific detectivity of 10^{14} Jones [9]. Sorifi *et al.*[57] fabricated a vertical p-n heterojunction photodetector using GaSe and Si. The device was characterized using Kelvin probe force microscopy (KPFM), revealing a type-II band alignment at the GaSe/Si heterojunction.

Current-voltage measurements demonstrated rectifying behaviour, with a high current rectification ratio of approximately 1000 at ± 5 V. The fabricated GaSe/Si photodiode exhibited exceptional photoresponse performance, with a high photoresponsivity, specific detectivity, and external quantum efficiency (EQE) value of approximately 2.8×10^{3} A/W, 6.2×10^{12} Jones, and 6011, respectively, at a biasing of −5V. Notably, a remarkable photoresponse of 6 AW^{-1} was achieved at zero bias, indicating self-driven operation without the need for external power. Pham *et al.*[58] conducted a comprehensive investigation using density functional theory to analyze the atomic structures and electronic properties of GaSe/MoS_2 and GaS/$MoSe_2$ heterojunctions. Their calculations revealed the presence of a type-II band alignment in both GaSe/MoS_2 and GaS/$MoSe_2$ heterojunctions. This significant finding suggests that these heterojunctions hold great promise for the fabrication and design of innovative photovoltaic and optoelectronic devices. It is crucial to emphasize that the development and understanding of Ga-based MMCs are currently advancing, and further research is necessary to comprehensively investigate their properties and potential applications. The structural versatility, layer-dependent electronic properties, and the current benchmarked performance of various Ga-based MMC heterojunction architectures are summarized in **Fig. 4.**

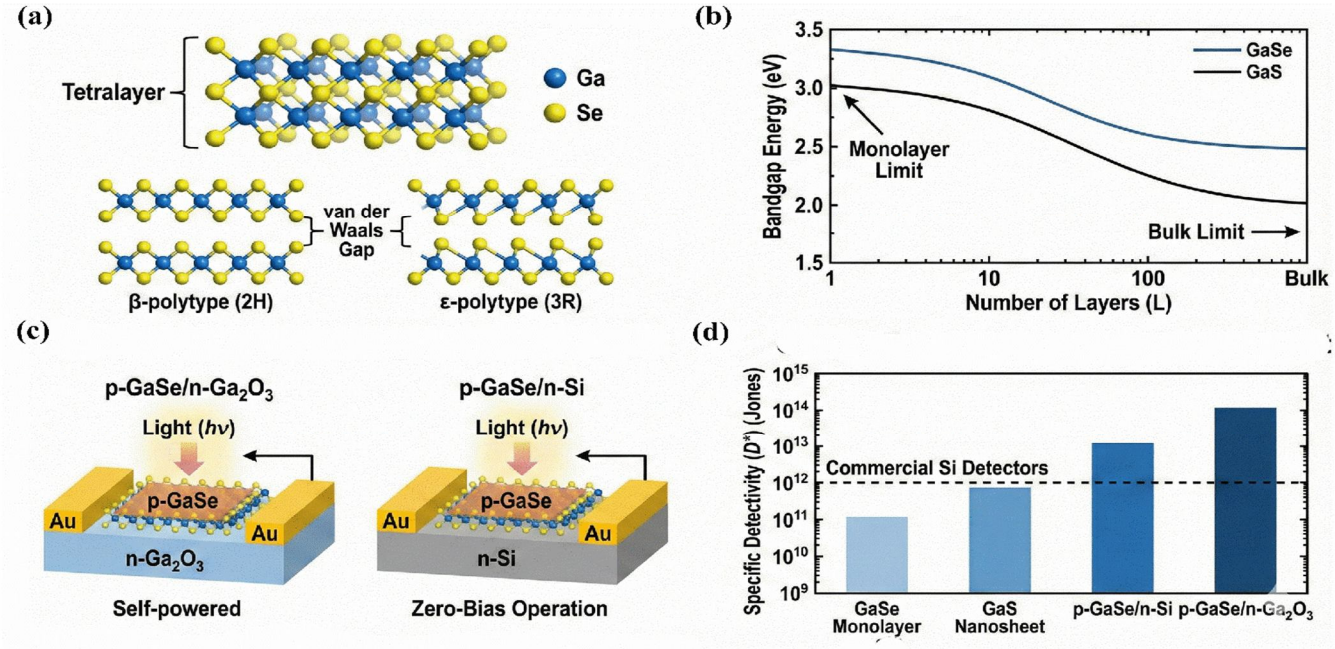

Fig. 4: Current technological status of Gallium-based MMCs. (a) Representative tetralayer atomic structure and common stacking polytypes. (b) Layer-dependent bandgap evolution illustrating the transition from bulk to the monolayer limit. (c) Schematic of high-performance p-n heterojunction architectures ($GaSe/Ga_2O_3$ and GaSe/Si) facilitating self-powered photodetection. (d) Comparative benchmarking of optoelectronic figures-of-merit for Ga-based 2D material systems.

VII. CONCLUSION

The emergence of two-dimensional Gallium-based metal monochalcogenides (MMCs) has established a new frontier in next-generation optoelectronics, effectively bridging the performance and bandgap limitations inherent to graphene and transition metal dichalcogenides (TMDCs). This review has systematically highlighted the unique intrinsic properties of GaSe and GaS, including their distinctive direct-to-indirect thickness-dependent bandgap transitions, exceptionally low carrier effective masses, and inherent p-type or solar-blind characteristics. By leveraging photoconductive, photogating, and photovoltaic sensing mechanisms, devices based on these materials have demonstrated remarkable optoelectronic figures-of-merit, achieving ultra-high specific detectivities (exceeding 10^{14} Jones) and massive external quantum efficiencies.

A defining advantage of Ga-based MMCs lies in their ultrafast interfacial charge dynamics and unprecedented stacking tunability. As elucidated through recent computational models and experimental transient absorption spectroscopy, the weak non-adiabatic coupling in these systems enables a substantial suppression of electron-hole recombination. Consequently, properly engineered van der Waals heterostructures—such as GaSe/GaTe, GaSe/Ga_2O_3, and GaSe/Si—can prolong photocarrier lifetimes by orders of magnitude compared to TMDC-only architectures. This interfacial mastery facilitates the realization of Type-II band alignments that drive highly efficient, self-powered photodetection at zero bias.

However, the transition of Ga-based MMC photodetectors from laboratory-scale prototypes to commercial optoelectronic integration faces critical engineering challenges. While significant progress has been made in top-down exfoliation and bottom-up synthesis methods (CVD, PVD, and PLD), achieving wafer-scale, single-crystalline uniformity with precise layer control remains a primary hurdle. Furthermore, mitigating surface defect densities and ensuring the long-term ambient stability of these atomically thin layers will require the development of robust defect-passivation and encapsulation strategies.

Moving forward, the synergistic combination of ab initio computational predictions (DFT and NAMD) with advanced time-resolved spectroscopy will be essential to rationally design optimal stacking registries and heterojunction interfaces. Future research paradigms should prioritize the integration of these high-gain, self-driven MMC sensors into flexible substrates, multispectral imaging arrays, and low-power logic circuits. Ultimately, Gallium-based metal monochalcogenides possess the transformative potential to redefine the operational limits of high-sensitivity, broadband, and wearable optoelectronic systems.

VIII. ACKNOWLEDGMENT

The author wishes to express his sincere gratitude to the Department of Physics, Godda College, under Sido-Kanhu Murmu University, for providing the essential academic environment, administrative support, and research infrastructure that facilitated the preparation of this comprehensive review. Deep appreciation is also extended to colleagues and peers whose insightful discussions significantly contributed to the comparative analyses of 2D metal monochalcogenides presented in this work.

Conflicts Of Interest

The author declare no conflicts of interest.

REFERENCES

[1] K. S. Novoselov et al., “Two-dimensional atomic crystals,” Proceedings of the National Academy of Sciences, vol. 102, no. 30, pp. 10451–10453, Jul. 2005.
[2] K. S. Novoselov, V. I. Fal′ko, L. Colombo, P. R. Gellert, M. G. Schwab, and K. Kim, “A roadmap for graphene,” Nature, vol. 490, no. 7419, pp. 192–200, Oct. 2012.
[3] R. Ganatra and Q. Zhang, “Few-Layer MoS 2 : A Promising Layered Semiconductor,” ACS Nano, vol. 8, no. 5, pp. 4074–4099, May 2014.
[4] J. D. Yao, Z. Q. Zheng, J. M. Shao, and G. W. Yang, “Stable, highly-responsive and broadband photodetection based on large-area multilayered WS 2 films grown by pulsed-laser deposition,” Nanoscale, vol. 7, no. 36, pp. 14974–14981, 2015.
[5] H. Huang et al., “Highly sensitive phototransistor based on GaSe nanosheets,” Applied Physics Letters, vol. 107, no. 14, p. 143112, Oct. 2015.
[6] G. Konstantatos and E. H. Sargent, “Nanostructured materials for photon detection,” Nature Nanotechnology, vol. 5, no. 6, pp. 391–400, Jun. 2010.
[7] D. V. Rybkovskiy et al., “Size-induced effects in gallium selenide electronic structure: The influence of interlayer interactions,” Physical Review B, vol. 84, no. 8, p. 085314, Aug. 2011.
[8] M. Zhao et al., “Advances in Two-Dimensional Materials for Optoelectronics Applications,” Crystals, vol. 12, no. 8, p. 1087, Aug. 2022.
[9] Y. Wang et al., “p -GaSe/ n -Ga 2 O 3 van der Waals Heterostructure Photodetector at Solar-Blind Wavelengths with Ultrahigh Responsivity and Detectivity,” ACS Photonics, vol. 8, no. 8, pp. 2256–2264, Aug. 2021.
[10] L. Dong et al., “Performance-enhanced solar-blind photodetector based on a CH 3 NH 3 PbI 3 /β-Ga 2 O 3 hybrid structure,” Journal of Materials Chemistry C, vol. 7, no. 45, pp. 14205–14211, 2019.
[11] P. Hu et al., “Highly Responsive Ultrathin GaS Nanosheet Photodetectors on Rigid and Flexible Substrates,” Nano Letters, vol. 13, no. 4, pp. 1649–1654, Apr. 2013.
[12] U. Varshney, A. Sharma, and G. Gupta, “Synthesis of GaSe nanoflorets for highly responsive and fast response self-powered visible photodetectors,” Journal of Materials Science: Materials in Electronics, vol. 36, no. 10, p. 619, Apr. 2025.
[13] C. Odaci, M. S. Khan, M. Jose, M. Kisielewska, A. Roshanghias, and U. Aydemir, “Degrading effect on electrical properties of printed gallium sulfide based photodetector,” Flexible and Printed Electronics, vol. 9, no. 2, p. 025010, Jun. 2024.
[14] S. Kaushik and R. Singh, “2D Layered Materials for Ultraviolet Photodetection: A Review,” Advanced Optical Materials, vol. 9, no. 11, p. 2002214, Jun. 2021.
[15] P. C. Y. Chow and T. Someya, “Organic Photodetectors for Next-Generation Wearable Electronics,” Advanced Materials, vol. 32, no. 15, p. 1902045, Apr. 2020.
[16] M. Buscema et al., “Photocurrent generation with two-dimensional van der Waals semiconductors,” Chemical Society Reviews, vol. 44, no. 11, pp. 3691–3718, 2015.
[17] C. Xie, C. Mak, X. Tao, and F. Yan, “Photodetectors Based on Two-Dimensional Layered Materials Beyond Graphene,” Advanced Functional Materials, vol. 27, no. 19, p. 1603886, May 2017.
[18] F. Wang et al., “2D library beyond graphene and transition metal dichalcogenides: a focus on photodetection,” Chemical Society Reviews, vol. 47, no. 16, pp. 6296–6341, 2018.
[19] M. Long, P. Wang, H. Fang, and W. Hu, “Progress, Challenges, and Opportunities for 2D Material Based Photodetectors,” Advanced Functional Materials, vol. 29, no. 19, p. 1803807, May 2019.
[20] X. Gong et al., “High-Detectivity Polymer Photodetectors with Spectral Response from 300 nm to 1450 nm,” Science, vol. 325, no. 5948, pp. 1665–1667, Sep. 2009.
[21] C. Xie, C. Mak, X. Tao, and F. Yan, “Photodetectors Based on Two-Dimensional Layered Materials Beyond Graphene,” Advanced Functional Materials, vol. 27, no. 19, p. 1603886, May 2017.

[22] X. Xiong, Q. Zhang, X. Zhou, B. Jin, H. Li, and T. Zhai, "One-step synthesis of p-type GaSe nanoribbons and their excellent performance in photodetectors and phototransistors," Journal of Materials Chemistry C, vol. 4, no. 33, pp. 7817–7823, 2016.
[23] G. H. Shin et al., "Si–MoS 2 Vertical Heterojunction for a Photodetector with High Responsivity and Low Noise Equivalent Power," ACS Applied Materials & Interfaces, vol. 11, no. 7, pp. 7626–7634, Feb. 2019.
[24] B. R. Tak, V. Gupta, A. K. Kapoor, Y.-H. Chu, and R. Singh, "Wearable Gallium Oxide Solar-blind Photodetectors on Muscovite Mica Having Ultra-High Photoresponsivity And Detectivity With Added High Temperature Functionalities," ACS Applied Electronic Materials, p. acsaelm.9b00603, 2019.
[25] X. C. Guo et al., "β -Ga 2 O 3 / p -Si heterojunction solar-blind ultraviolet photodetector with enhanced photoelectric responsivity," Journal of Alloys and Compounds, vol. 660, pp. 136–140, Mar. 2016.
[26] Y. Lu et al., "GaS:WS 2 Heterojunctions for Ultrathin Two-Dimensional Photodetectors with Large Linear Dynamic Range across Broad Wavelengths," ACS Nano, vol. 15, no. 12, pp. 19570–19580, Dec. 2021.
[27] N. Curreli et al., "Liquid Phase Exfoliated Indium Selenide Based Highly Sensitive Photodetectors," Advanced Functional Materials, vol. 30, no. 13, p. 1908427, Mar. 2020.
[28] J. N. Coleman et al., "Two-Dimensional Nanosheets Produced by Liquid Exfoliation of Layered Materials," Science, vol. 331, no. 6017, pp. 568–571, Feb. 2011.
[29] S. Lei et al., "Synthesis and Photoresponse of Large GaSe Atomic Layers," Nano Letters, vol. 13, no. 6, pp. 2777–2781, Jun. 2013.
[30] N. T. Shelke and B. R. Karche, "Hydrothermal synthesis of WS2/RGO sheet and their application in UV photodetector," Journal of Alloys and Compounds, vol. 653, pp. 298–303, 2015.
[31] F. Liu et al., "High-Sensitivity Photodetectors Based on Multilayer GaTe Flakes," ACS Nano, vol. 8, no. 1, pp. 752–760, Jan. 2014.
[32] S. R. Tamalampudi et al., "High Performance and Bendable Few-Layered InSe Photodetectors with Broad Spectral Response," Nano Letters, vol. 14, no. 5, pp. 2800–2806, May 2014.
[33] P. Hu, Z. Wen, L. Wang, P. Tan, and K. Xiao, "Synthesis of Few-Layer GaSe Nanosheets for High Performance Photodetectors," ACS Nano, vol. 6, no. 7, pp. 5988–5994, Jul. 2012.
[34] S. Yang et al., "High performance few-layer GaS photodetector and its unique photo-response in different gas environments," Nanoscale, vol. 6, no. 5, pp. 2582–2587, 2014.
[35] N. Curreli et al., "Liquid Phase Exfoliated Indium Selenide Based Highly Sensitive Photodetectors," Advanced Functional Materials, vol. 30, no. 13, p. 1908427, Mar. 2020.
[36] A. S. Chan, X. Fu, G. N. Panin, H. D. Cho, D. J. Lee, and T. W. Kang, "Shear Exfoliation and Photoresponse of 2D-Layered Gallium Selenide Nanosheets," physica status solidi (RRL) - Rapid Research Letters, vol. 12, no. 10, p. 1800226, Oct. 2018.
[37] J. Zhou et al., "Controlled Synthesis of High-Quality Monolayered α-In 2 Se 3 via Physical Vapor Deposition," Nano Letters, vol. 15, no. 10, pp. 6400–6405, Oct. 2015.
[38] Y. Zhou et al., "Epitaxy and Photoresponse of Two-Dimensional GaSe Crystals on Flexible Transparent Mica Sheets," ACS Nano, vol. 8, no. 2, pp. 1485–1490, Feb. 2014.
[39] D. Ruzmetov et al., "Vertical 2D/3D Semiconductor Heterostructures Based on Epitaxial Molybdenum Disulfide and Gallium Nitride," ACS Nano, vol. 10, no. 3, pp. 3580–3588, Mar. 2016.
[40] M. Sharma, A. Singh, and R. Singh, "Monolayer MoS 2 Transferred on Arbitrary Substrates for Potential Use in Flexible Electronics," ACS Applied Nano Materials, vol. 3, no. 5, pp. 4445–4453, May 2020.
[41] X. Li et al., "Controlled Vapor Phase Growth of Single Crystalline, Two-Dimensional GaSe Crystals with High Photoresponse," Scientific Reports, vol. 4, no. 1, p. 5497, May 2015.
[42] H.-C. Chang et al., "Synthesis of Large-Area InSe Monolayers by Chemical Vapor Deposition," Small, vol. 14, no. 39, p. 1802351, Sep. 2018.
[43] J. D. Yao, Z. Q. Zheng, and G. W. Yang, "Production of large-area 2D materials for high-performance photodetectors by pulsed-laser deposition," Progress in Materials Science, vol. 106, no. January 2018, p. 100573, 2019.
[44] M. Mahjouri-Samani et al., "Digital Transfer Growth of Patterned 2D Metal Chalcogenides by Confined Nanoparticle Evaporation," ACS Nano, vol. 8, no. 11, pp. 11567–11575, Nov. 2014.
[45] Z. Li et al., "Van Der Waals Vertical GaSe/MoS2 Heterojunctions for High-responsivity Photodetectors and Sensitive Photovoltaic Devices," Innovation Discovery, vol. 1, no. 1, p. 3, Mar. 2024.
[46] Z. Li et al., "Van Der Waals Vertical GaSe/MoS2 Heterojunctions for High-responsivity Photodetectors and Sensitive Photovoltaic Devices," Innovation Discovery, vol. 1, no. 1, p. 3, Mar. 2024.
[47] V. Kumar, P. Kumar, Akash, A. Saini, and J. S. Gwag, "Tunable Electronic, Optoelectronic, and Photocatalytic Properties of MoS 2 and GaS Monolayers in the MoS 2 /GaS Heterostructure," ChemistrySelect, vol. 9, no. 37, Oct. 2024.
[48] Y. Ma, A. Bao, X. Guo, and J. Wang, "Carrier mobility and optical properties of a type-II GaSe/ZnS heterostructure as a photocatalyst: a first-principles study," Physical Chemistry Chemical Physics, vol. 26, no. 20, pp. 14980–14990, 2024.
[49] Q. Liu et al., "Exploring tunable optoelectronic properties of two-dimensional GaS/PtSSe heterostructures under biaxial strain and external electric field," Computational and Theoretical Chemistry, vol. 1240, p. 114839, Oct. 2024.
[50] Z. Yan et al., "Dramatically Prolonged Photoexcited Carrier Lifetimes in Group-III Monochalcogenide Heterostructures through Stacking Modulation," The Journal of Physical Chemistry Letters, vol. 16, no. 17, pp. 4286–4295, May 2025.
[51] A. Soni, S. Ghosal, M. Kundar, S. K. Pati, and S. K. Pal, "Long-Lived Interlayer Excitons in WS 2 /Ruddlesden–Popper Perovskite van der Waals Heterostructures," ACS Applied Materials & Interfaces, vol. 16, no. 27, pp. 35841–35851, Jul. 2024.
[52] E. Blundo et al., "Giant Light Emission Enhancement in Strain-Engineered InSe/MS 2 (M = Mo or W) van der Waals Heterostructures," Nano Letters, vol. 25, no. 9, pp. 3375–3382, Mar. 2025.
[53] C. Wang et al., "Weakening of the Many-Body Interactions Induced by Charge Transfer in Gr/WS 2 Heterostructures," The Journal of Physical Chemistry C, vol. 128, no. 22, pp. 9209–9216, Jun. 2024

[54] N. Rafizadeh, G. Agunbiade, R. J. Scott, M. Vieux, and H. Zhao, "Type-I and type-II interfaces in a MoSe2/WS2 van der Waals heterostructure," Applied Physics Letters, vol. 126, no. 4, Jan. 2025.
[55] V. Augelli, C. Manfredotti, R. Murri, and L. Vasanelli, "Hall-mobility anisotropy in GaSe," Physical Review B, vol. 17, no. 8, pp. 3221–3226, Apr. 1978
[56] S. Sorifi, M. Moun, S. Kaushik, and R. Singh, "High-Temperature Performance of a GaSe Nanosheet-Based Broadband Photodetector," ACS Applied Electronic Materials, vol. 2, no. 3, pp. 670–676, Mar. 2020.
[57] S. Sorifi, S. Kaushik, and R. Singh, "A GaSe/Si-based vertical 2D/3D heterojunction for high-performance self-driven photodetectors," Nanoscale Advances, vol. 4, no. 2, pp. 479–490, 2022.
[58] K. D. Pham, H. V. Phuc, N. N. Hieu, B. D. Hoi, and C. V. Nguyen, "Electronic properties of GaSe/MoS 2 and GaS/MoSe 2 heterojunctions from first principles calculations," AIP Advances, vol. 8, no. 7, p. 075207, Jul. 2018.

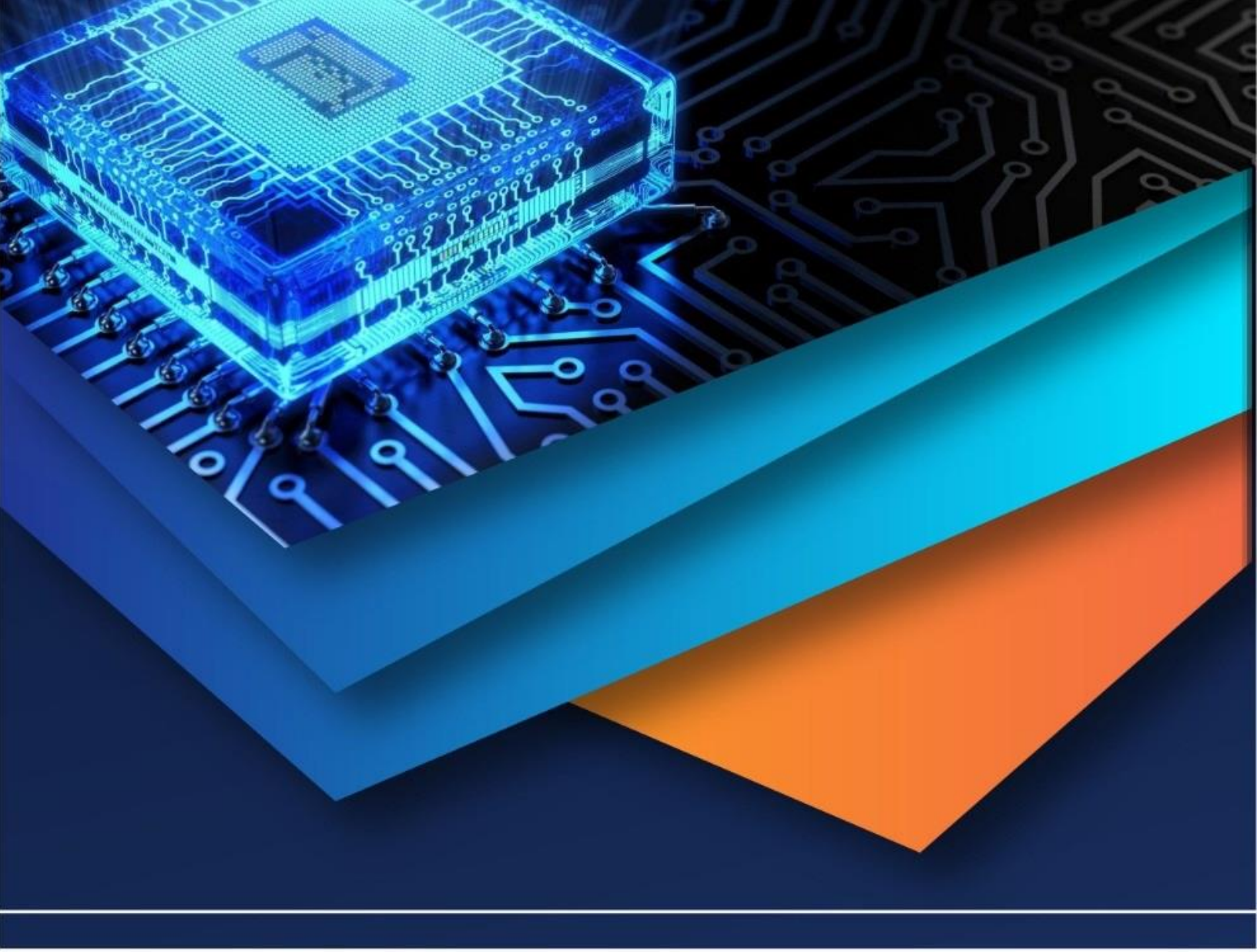

10.22214/IJRASET

45.98

IMPACT FACTOR: 7.129

IMPACT FACTOR: 7.429

INTERNATIONAL JOURNAL FOR RESEARCH

IN APPLIED SCIENCE & ENGINEERING TECHNOLOGY